# Thermal equation of state of polarized fermions in one dimension via complex chemical potentials

Andrew C. Loheac,[1] Jens Braun,[2] Joaquín E. Drut,[1] and Dietrich Roscher[2]

[1] *Department of Physics and Astronomy, University of North Carolina, Chapel Hill, North Carolina 27599, USA*
[2] *Institut für Kernphysik (Theoriezentrum), Technische Universität Darmstadt, D-64289 Darmstadt, Germany*

We present a nonperturbative computation of the equation of state of polarized, attractively interacting, nonrelativistic fermions in one spatial dimension at finite temperature. We show results for the density, spin magnetization, magnetic susceptibility, and Tan's contact. We compare with the second-order virial expansion, a next-to-leading-order lattice perturbation theory calculation, and interpret our results in terms of pairing correlations. Our lattice Monte Carlo calculations implement an imaginary chemical potential difference to avoid the sign problem. The thermodynamic results on the imaginary side are analytically continued to obtain results on the real axis. We focus on an intermediate- to strong-coupling regime, and cover a wide range of temperatures and spin imbalances.

## I. INTRODUCTION

In the last two decades, experimental studies with ultracold atomic gases have made consistent strides towards the increasingly clean and controlled characterization of strongly coupled matter, particularly in nonperturbative regimes that are out of reach for conventional theory methods [1]. This represents a challenge to the theory side, which has been met in some cases but remains open in general.

As is well known, spatial dimensionality plays a crucial role in these systems regardless of the strength of the interaction. Although it is also generally understood that interactions tend to dominate in lower dimensions and, conversely, mean-field descriptions become more reliable in higher dimensions, they in general do not allow for quantitative predictions. This can be viewed as a signal that fluctuation effects still play a prominent role, calling for more sophisticated theoretical tools. Both from the theory and experiment sides, considerable progress has been made in the study of three-dimensional (3D) systems in a variety of situations (e.g., in harmonic traps, homogeneous space, polarized, unpolarized, in the ground state, at finite temperature, etc.; see Ref. [2] for reviews), in particular with emphasis on the so-called BEC-BCS crossover and scale-invariant regimes [3], as well as the Efimov effect [4]. In recent years, there has also been increasing activity in similar studies in 2D (see, e.g., Ref. [5] for a recent review), where the possibility of accessing directly the superfluid Berezinskii-Kosterlitz-Thouless transition [6] has been a major drive.

In this context, the motivation to study one-dimensional systems, in particular fermions, is manifold. Large classes of 1D problems can be solved exactly at zero temperature via powerful techniques such as the Bethe ansatz, which has propelled a fair amount of work over the last few decades (see, e.g., Refs. [7, 8]). However, a new wave of interest has been underway for a few years. This renewed activity stems in part from the realization of 1D systems in the form of atomic gases in highly constrained, quasi-1D optical traps, but it is also due to the advent of quantum-information concepts in condensed-matter physics [9] and their connection to quantum phase transitions (in particular topological ones) in low dimensions.

Systems of spin-polarized, attractively interacting fermions are particularly appealing because of the potential occurrence of spontaneously broken translation invariance in exotic superfluid phases [10]. The focus of the present work, however, is on the basic thermodynamic equations of state of spin-polarized fermions in 1D, rather than on detecting potential exotic superfluid phases. We compute the density and the spin magnetization as well as Tan's contact, which encodes the importance of high-momentum correlations in systems with short-range interactions [11, 12]. Our study is distinguished from previous ones in that we make use of complex chemical potentials to overcome the so-called sign problem. The latter has been a major roadblock in lattice Monte Carlo calculations of asymmetric systems (e.g., systems with mass or spin imbalance [13, 14], or at finite quark density in the case of QCD [15]), as explained below. As a proof of principle, we consider spin-1/2 fermions in 1D with attractive contact interactions, but more general situations including richer interactions and higher dimensions can be studied with the same methods. Note that we do not determine the exact nature of the ground state of the theory in our present study; as we explain in detail below, our approach based on complex chemical potentials is in fact unable to reach the ground state (and at fixed temperature is not able to reach arbitrary polarizations). Nevertheless, the ground state indirectly leaves its imprint in our computation of the basic thermodynamic equations of state.

The Hamiltonian we analyze is that of the Gaudin-Yang model [16],

$$\hat{H} = -\frac{\hbar^2}{2m}\sum_i \nabla_i^2 - \sum_{i<j} g\delta(x_i - x_j), \tag{1}$$

where the sums are over all particles. In our study, we will consider polarized systems, in the sense that they will have a nonvanishing average spin magnetization in

general. In the grand-canonical ensemble, the partition function of such a system is

$$\mathcal{Z}(\beta\mu_\uparrow, \beta\mu_\downarrow) = \mathrm{Tr}\exp\left[-\beta(\hat{H} - \mu_\uparrow\hat{N}_\uparrow - \mu_\downarrow\hat{N}_\downarrow)\right], \quad (2)$$

where $\mu_s$ is the chemical potential for spin $s =\uparrow,\downarrow$ particles, $\hat{N}_s$ is the corresponding particle number operator, and $\beta$ is the inverse temperature.

As mentioned above, asymmetric systems are challenging for lattice Monte Carlo calculations due to the appearance of the sign problem. To circumvent this difficulty, we implement the approach put forward in Ref. [13]. Here we attempt this type of calculation for a nonrelativistic theory; a similar strategy has been applied by some of the present authors to ground-state calculations in the mass-imbalanced case [14]. In the present case, we take the chemical potential for each fermion species to be complex, but such that one is the complex conjugate of the other: $\mu_\uparrow = \mu_\downarrow^*$. As a consequence, the fermion determinants in the Monte Carlo calculation (see, e.g., Ref. [14, 17]) are also complex conjugates of one another, and the probability measure is thus nonnegative.

In this approach, the overall chemical potential $\mu = (\mu_\uparrow + \mu_\downarrow)/2$ is real, as usual, but the asymmetry parameter $h = (\mu_\uparrow - \mu_\downarrow)/2$ is imaginary. For convenience, we define $h_\mathrm{I} := \mathrm{Im}\, h = -ih$, with $h_\mathrm{I}$ being a real-valued number. The total density $n = n_\uparrow + n_\downarrow$ in our study based on the grand-canonical ensemble is then still a real-valued number, while the so-called spin magnetization $m = n_\uparrow - n_\downarrow$ is imaginary. These, as well as every output of the calculation, must be analytically continued to the real-$h$ axis in order to obtain the physical results. While the analytic continuation procedure introduces some degree of arbitrariness in the final results (see below), it should be pointed out that the results on the imaginary side are fully nonperturbative and, in principle, exact, and certain aspects of the functional dependence with respect to $h$ are known. Note, for instance, that the asymmetry $h$ always enters in the calculations as a function of $\beta h$. Moreover, it can be shown that the results for imaginary asymmetries will be $2\pi$ periodic in $\beta h_\mathrm{I}$; see Ref. [13]. This is therefore a compact parameter and we will restrict it to the interval $[-\pi, \pi]$. The symmetry in the form of the partition function under spin exchange indicates that the physics it describes is independent of the sign of $h$, i.e., we expect our results to be either odd or even functions of $h$, depending on the observable.

We would like to emphasize that although it is, in principle, exact, our present Monte Carlo approach to spin-imbalanced Fermi gases is not capable of studying the zero-temperature limit, but is limited to finite temperatures $|\beta h_\mathrm{I}| \leq \pi$ being a direct consequence of the $2\pi$ periodicity in $\beta h_\mathrm{I}$. For the same reason, one may say that at fixed temperature (i.e. $\beta$) not all polarizations are achievable, as the above constraint limits the range of $h_\mathrm{I}$. In this sense, our present approach is complementary to the *Bethe* ansatz [7, 8] which allows for an exact solution of one-dimensional Fermi gases in the zero-temperature limit. Still, our approach enables us to compute the finite-temperature equation of state in a certain parameter range which can then potentially be compared to experiments, see, e.g., Ref. [18]. The present, however, should rather be regarded as a proof-of-principle work that serves as an intermediate step towards calculations in higher dimensions.

It should also be pointed out that we do not expect phase transitions to be present in this 1D system as a function of temperature due to the absence of spontaneous symmetry breaking [19]. This fact should allow for a more reliable analytic continuation from $\beta h_\mathrm{I}$ to the real side. Conversely, the appearance of accumulation points of zeros of the partition function (the so-called Yang-Lee zeros) in higher dimensions may complicate the analytic continuation in those cases.

## II. SCALES AND COMPUTATIONAL TECHNIQUE

### A. General setup

The problem of fermions with a contact interaction is ultraviolet-finite in one spatial dimension. Therefore, the bare coupling has a physical meaning: in the continuum limit, $g = 2/a_0$, where $a_0$ is the scattering length for the symmetric channel (see e.g. [20]); accordingly, $g$ will be reported in units of $\sqrt{\beta}$. Note that the thermal de Broglie wavelength is $\lambda_T = \sqrt{2\pi\beta}$.

To characterize the thermodynamics of polarized interacting fermions in one dimension we compute three quantities, namely the density $n$, the spin magnetization $m$ and the contact $C$, as functions of the inverse temperature $\beta$, the average chemical potential $\mu$, the chemical potential difference $h$, and the coupling $g$. To make all of these quantities dimensionless, we utilize the noninteracting unpolarized density $n_0$ as the scale for $n$ and $m$, i.e. we report $n/n_0$ and $m/n_0$. On the other hand, for the input parameters we set $\beta$ as the main scale, i.e. we report the physical results as functions of

$$\beta\mu, \quad \beta h, \quad \text{and} \quad \lambda \equiv \sqrt{\beta}g\,, \quad (3)$$

where the contact $C$ is made dimensionless by $C_0$, the unpolarized result at $\beta\mu = 0$. Note that, since we use an imaginary chemical potential difference in our Monte Carlo studies, the "bare" outcome of these simulations will be given as a function of $\beta\mu$, $\beta h_\mathrm{I}$, and $\lambda$.

From the density and the magnetization one may obtain the isothermal compressibility and magnetic susceptibility simply by taking derivatives with respect to $\beta\mu$ and $\beta h$, respectively. Mixed response functions (of $n$ with respect to $\beta h$, or $m$ with respect to $\beta\mu$) may be obtained in the same fashion. On the other hand, numerical integration of $n$ with respect to $\beta\mu$ provides the pressure for each value of $\beta h$.

The computational method utilized in this work is very similar to the one of Refs. [21–23], but reduced to one spatial dimension and generalized to complex chemical potentials as explained above (see also Ref. [24]). Because one-dimensional problems are computationally inexpensive, it is possible to calculate in very large lattices, e.g. $N_x \sim \mathcal{O}(10^2)$. For such sizes, the continuum limit is easily achieved by lowering the density, while still remaining in the many-particle (i.e. thermodynamic) regime. For the proof-of-principle calculations presented here, we fix $\lambda = 1.0$. This was chosen as being in the intermediate-to-strong-coupling regime, which is typically outside the range of validity of perturbative approaches. For such a coupling strength, a lattice size of $N_x = 61$, which we fixed throughout this study, is sufficient to provide a good quantitative understanding of the continuum limit (see Ref. [24]). The physical extent of the system is $L = N_x \ell$, where $\ell = 1$ fixes the spatial lattice units. The extent of the temporal lattice is given by $\beta = \tau N_\tau$, where we take $\tau = 0.05/\ell^2$.

### B. Computing the density and magnetization at imaginary asymmetry

At imaginary chemical potential asymmetry, the partition function of Eq. (2) can be written in terms of a Hubbard-Stratonovich auxiliary field $\sigma$ as

$$\mathcal{Z} = \int \mathcal{D}\sigma |\det(1 + zU[\sigma])|^2 \,, \tag{4}$$

where $z \equiv z_\uparrow = \exp(\beta\mu_\uparrow) = \exp(\beta\mu_\downarrow^*) = z_\downarrow^*$, and $U[\sigma]$ is a matrix that encodes the dynamics of the system (see e.g. Ref. [17]). We thus identify

$$P[\sigma] \equiv |\det(1 + zU[\sigma])|^2 \tag{5}$$

as the non-negative probability measure for our Monte Carlo calculations. The total (average) particle density $n$ is then obtained in those calculations using

$$n = \frac{1}{L}\frac{\partial \ln \mathcal{Z}}{\partial(\beta\mu)} = \frac{2}{\mathcal{Z}L}\int \mathcal{D}\sigma P[\sigma] \mathrm{Re}\left[\mathrm{Tr}\left(\frac{zU[\sigma]}{1 + zU[\sigma]}\right)\right], \tag{6}$$

and the (average) spin magnetization $m$ can similarly be calculated using $m = (1/L)\partial \ln \mathcal{Z}/\partial(\beta h)$. To circumvent the sign problem in our Monte Carlo simulations, however, we rather compute

$$m = \frac{1}{L}\frac{\partial \ln \mathcal{Z}}{\partial(\beta h_\mathrm{I})} = -\frac{2i}{\mathcal{Z}L}\int \mathcal{D}\sigma P[\sigma] \mathrm{Im}\left[\mathrm{Tr}\left(\frac{zU[\sigma]}{1 + zU[\sigma]}\right)\right]. \tag{7}$$

Since we assume that $m$ is analytic as a function of general complex-valued $h$, at least in a finite domain about $h = 0$, we shall use the same label as for the physical spin magnetization.

To determine the contact, we use the same approach as in Ref. [24]. The definition in 1D is

$$C \equiv \frac{2}{\beta\lambda_T}\left.\frac{\partial(\beta\Omega)}{\partial(a_0/\lambda_T)}\right|_{\mu,T}, \tag{8}$$

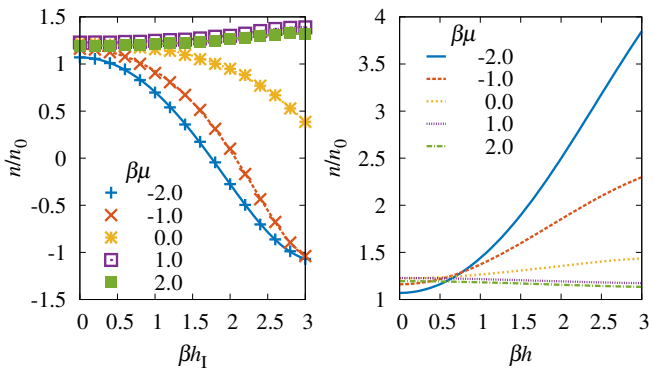


Figure 1. (Color online) Left: Density as a function of the imaginary chemical potential difference $\beta h_\mathrm{I}$ at various values of $\beta\mu$ for a dimensionless coupling of $\lambda = 1.0$. Right: Analytic continuation of the density as a function of $\beta h$ at various values of $\beta\mu$. In both plots the density is an even function about the origin and is plotted in units of the density of the noninteracting, unpolarized system.

where $\Omega = -\frac{1}{\beta}\ln \mathcal{Z}$ is the grand thermodynamic potential. Using the Feynman-Hellman theorem, it can be shown that

$$C = -g\langle \hat{V} \rangle, \tag{9}$$

where $\langle \hat{V} \rangle$ is the thermal expectation value of the interaction operator. The latter can be computed in Monte Carlo calculations using derivatives of $\ln \mathcal{Z}$ with respect to the bare lattice coupling $g$ or the lattice spacing $\tau$.

## III. RESULTS

### A. Monte Carlo results for imaginary asymmetry

Throughout this work, we present Monte Carlo calculations at $\beta = 8.0$ and a lattice size of $N_x = 61$. For the purposes of demonstrating the method, we fix the dimensionless coupling to $\lambda = 1.0$, although a variety of coupling strengths may also be explored using the same technique. The imaginary asymmetry parameter $\beta h_\mathrm{I}$ was varied over a full period $[-\pi, \pi]$, and the chemical potential parameter $\beta\mu$ was varied in the interval $[-4.0, 4.0]$, covering the semiclassical regime (where the virial expansion is valid) to the fully quantum mechanical regime. For each point in the plots below, we have taken 1000 de-correlated Monte Carlo samples, thus ensuring that the statistical uncertainty is below 10%.

In Fig. 1 we show the density as a function of $\beta h_\mathrm{I}$ and $\beta h$, respectively, for representative values of $\beta\mu$. Similarly, Fig. 2 displays the magnetization and Fig. 3 shows Tan's contact. The statistical error of the Monte Carlo calculations on the imaginary side is estimated to be on the order of the symbol size in all three figures. In all cases we show the Monte Carlo results at $\beta h_\mathrm{I}$ on the

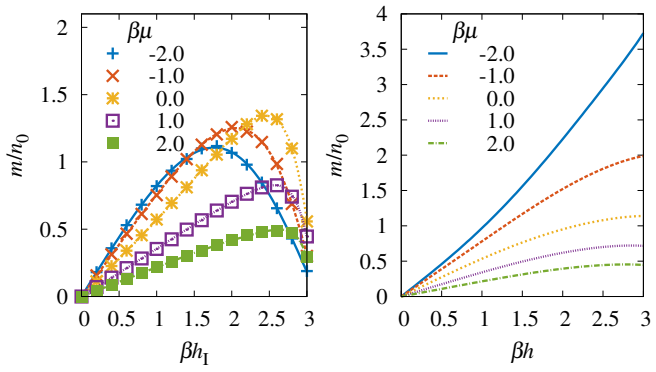


Figure 2. (Color online) Left: Magnetization as a function of the imaginary chemical potential difference $\beta h_{\rm I}$ at various values of $\beta\mu$ for a dimensionless coupling of $\lambda = 1.0$. Right: Analytic continuation of the magnetization as a function of $\beta h$ at various values of $\beta\mu$. In both plots the magnetization is an odd function about the origin and is plotted in units of the density of the noninteracting, unpolarized system.

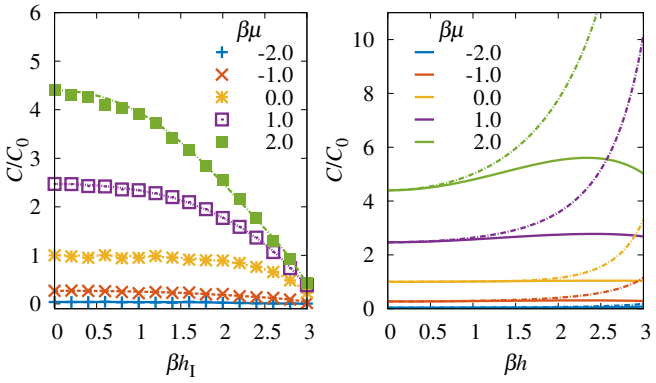


Figure 3. (Color online) Left: Tan's contact as a function of the imaginary chemical potential difference $\beta h_{\rm I}$ at various values of $\beta\mu$ for a dimensionless coupling of $\lambda = 1.0$. $C_0$ is the contact at $\beta h = \beta\mu = 0$. Right: Analytic continuation of the contact as a function of $\beta h$ at various values of $\beta\mu$. In both plots the contact is an even function about the origin. The curves on the right are color-wise paired by their value of $\beta\mu$, which coincides with the value on the left (by color code, or from top to bottom). Dashed-dotted lines give the results from a fit of the data to the polynomial-type ansatz (16), whereas solid lines result from fits of the data to our Padé-type ansatz (14) for the fit functions.

left panel, and the corresponding analytic continuation (described in detail below) on the right. Although the imaginary side of the problem is not physically meaningful, the results are non-perturbative, and it is reassuring that the data falls on smooth curves that respect the even or odd symmetry around $\beta h_{\rm I} = 0$. We therefore display only the positive interval $\beta h_{\rm I} \in [0, \pi]$.

### B. Analytic continuation to the real axis

In order to obtain the results of physical interest, we need to analytically continue the data from our Monte Carlo study to real-valued chemical potential differences. To this end, we fit our data to a specific ansatz for, e.g., the spin magnetization. Clearly, this is a critical step as the functional form of the ansatz is *a priori* unknown. However, as already discussed above, we know that, depending on the observable, the ansatz must be either an odd or even function in $\beta h_{\rm I}$ and that the partition function is periodic in $\beta h_{\rm I}$. Moreover, the virial expansion of the partition function $\mathcal{Z}$ suggests that $\mathcal{Z}$ can be written as a (asymptotic) series in powers of $\cos(\beta h_{\rm I})$, see also our discussion in Sect. IV. From such an analysis of the virial expansion, it also follows that higher-order terms in $\cos(\beta h_{\rm I})$ become particularly important for $\beta\mu \gg 1$. In order to take such higher order terms effectively into account, an ansatz of the type

$$\sim \frac{1}{1+\cos(\beta h_{\rm I})} \tag{10}$$

may be considered appropriate as it can be rewritten as an asymptotic series in powers of $\cos(\beta h_{\rm I})$, which still obeys the periodicity in $\beta h_{\rm I}$. An ansatz of this type may be viewed as a *Padé* approximant of cosines.

To be specific, we choose to fit our Monte Carlo data for the magnetization at finite $\beta h_{\rm I}$ with the function

$$f(\beta h_{\rm I}) = -i\frac{\mathcal{A}\sin(\beta h_{\rm I})}{1+\mathcal{B}\cos(\beta h_{\rm I})+\mathcal{C}F(\beta h_{\rm I})} \tag{11}$$

where $\mathcal{A}$, $\mathcal{B}$, and $\mathcal{C}$ are free real-valued fit parameters and the function $F$ is given by

$$F(x) = \cos\left(x^3/\pi^2\right). \tag{12}$$

Note that this last function has been found empirically. As written, it is analytic on the whole complex plane, in particular on a disk of radius $\pi$ centered at the origin. However, it is not periodic in $\beta h_{\rm I}$, as we required above. Here, we have indeed given up this constraint as we found that a large number of fit parameters is required to meet this criterion, rendering the fitting algorithm potentially unstable. For example, an ansatz of the form $\sim \sum_{k=1}\mathcal{A}_k\sin(k\beta h_{\rm I})/(1+\sum_{k=1}\mathcal{B}_k\cos(k\beta h_{\rm I}))$ is compatible with the above-mentioned constraints. However, the fit is of much lower quality than those obtained using Eq. (11). Interestingly, the parameter $\mathcal{C}$ associated with the function $F$ is in most cases found to be small when we fit our Monte Carlo data with the ansatz (11), see Tab. II.

The analytic continuation $\tilde{f}(\beta h)$ of Eq. (11) is obtained simply by setting $h_{\rm I} = -ih$, and is therefore given by

$$\tilde{f}(\beta h) = -\frac{\mathcal{A}\sinh(\beta h)}{1+\mathcal{B}\cosh(\beta h)+\mathcal{C}\tilde{F}(\beta h)}, \tag{13}$$

where $\tilde{F}$ is the analytic continuation of $F$.

In the case of the density and the contact, on the other hand, we expect even functions of $\beta h_{\rm I}$, and therefore we have chosen to fit the function

$$g(\beta h_{\rm I}) = \gamma \left[ \frac{1 + \mathcal{A}\eta(\beta h_{\rm I})}{1 + \mathcal{B}\eta(\beta h_{\rm I}) + \mathcal{C}\eta((\beta h_{\rm I})^3/\pi^2)} \right], \qquad (14)$$

where $\eta(x) = 1 - \cos(x)$. Here, $\gamma$ is a parameter that is fixed by the exactly known value at $\beta h = \beta h_{\rm I} = 0$, while $\mathcal{A}$, $\mathcal{B}$ and $\mathcal{C}$ are free real-valued fit parameters. Once the parameters are obtained, the analytic continuation $\tilde{g}(\beta h)$ of Eq. (14) is given by

$$\tilde{g}(\beta h) = \gamma \left[ \frac{1 + \mathcal{A}\tilde{\eta}(\beta h)}{1 + \mathcal{B}\tilde{\eta}(\beta h) + \mathcal{C}\tilde{\eta}((\beta h)^3/\pi^2)} \right], \qquad (15)$$

where $\tilde{\eta}(x) = 1 - \cosh(x)$.

The fit parameters for the density, magnetization, and Tan's contact are provided in Tables I, II, and III, respectively. Since the fits to the Monte Carlo data are sensitive to initial parameter values, the fitting algorithm performs several such fits with random initial parameter values in the interval $[-1, 1]$, and the best fit with the minimum mean residuals is chosen for the analytic continuation. Given the functional form of Eqs. (11) and (14), one should consider that poles may appear in either the fit or analytic continuation for a given set of fit parameters. Since we expect these quantities to be analytic for one dimensional Fermi gases,[1] the fitting algorithm eliminates any fits that demonstrate such behavior. Of course other functional forms may be considered for the analytic continuation with consideration to the constraints discussed.

In Fig. 1 we also show the analytic continuation of the density, in Fig. 2 of the magnetization, and in Fig. 3 of Tan's contact to real-valued chemical potential differences. Although these functions are not periodic in $\beta h$, they remain valid only in the original restricted domain of $[-\pi, \pi]$. A few representative values of $\beta\mu$ are shown in Figs. 1, 2, and 3, however such analytic continuations may be performed for many values of $\beta\mu$ on an unrestricted domain, and the equations of state for various imaginary asymmetries may be constructed. Such plots for representative values of $\beta h$ at a dimensionless coupling strength of $\lambda = 1.0$ for the density, magnetization, and Tan's contact are shown in Section IV B.

One of the most interesting features we observe in our results is the behavior of the magnetization $m/n_0$ as a function of $\beta h$ and $\beta\mu$. On the imaginary side (at least in the region studied), this quantity is non-monotonic in both of those variables. In particular, we note that the ordering of the curves, for different values of $\beta\mu$, is partially inverted at large enough $\beta h$. This behavior, however, results in a perfectly ordered set of curves on the real-valued ($\beta h$) side, in a way that respects both thermodynamic stability and physical intuition.

Table I. Fit parameters for the density as they appear in Eq. (14) at a constant dimensionless coupling of $\lambda = 1.0$ for various values of $\beta\mu$, as well as the $\chi^2$ per degree of freedom for each fit. Note that $\gamma$ is not a fit parameter (see main text). The value in parentheses indicates the calculated uncertainty of the least significant digit for each fit parameter.

| $\beta\mu$ | $\gamma$ | $\mathcal{A}$ | $\mathcal{B}$ | $\mathcal{C}$ | $\chi^2$ |
|---|---|---|---|---|---|
| -3.6 | 1.0080 | -0.9670(4) | -0.041(1) | -0.001(1) | 0.71 |
| -3.2 | 1.0172 | -0.9511(4) | -0.0565(9) | -0.002(1) | 0.58 |
| -2.8 | 1.0294 | -0.9281(4) | -0.080(1) | -0.006(1) | 0.54 |
| -2.4 | 1.0461 | -0.8942(9) | -0.118(3) | 0.005(3) | 1.29 |
| -2.0 | 1.0698 | -0.848(1) | -0.156(3) | -0.000(4) | 1.66 |
| -1.6 | 1.1026 | -0.7904(6) | -0.198(2) | -0.016(2) | 0.35 |
| -1.2 | 1.1245 | -0.716(1) | -0.276(3) | -0.008(4) | 1.25 |
| -0.8 | 1.1731 | -0.6334(6) | -0.323(2) | -0.019(3) | 0.63 |
| -0.4 | 1.1921 | -0.5433(9) | -0.364(4) | -0.034(7) | 1.30 |
| 0.0 | 1.2240 | -0.492(2) | -0.415(2) | -0.056(5) | 2.74 |
| 0.4 | 1.2359 | -0.503(3) | -0.493(3) | -0.009(1) | 5.21 |
| 0.8 | 1.2361 | -0.4(1) | -0.4(1) | 0.00(1) | 0.54 |
| 1.2 | 1.2214 | -0.18(5) | -0.22(5) | -0.013(6) | 0.97 |
| 1.6 | 1.2109 | -0.32(2) | -0.34(2) | 0.004(1) | 0.71 |
| 2.0 | 1.1948 | -0.33(3) | -0.35(3) | 0.005(2) | 1.81 |
| 2.4 | 1.1763 | -0.22(2) | -0.24(2) | -0.002(1) | 0.41 |
| 2.8 | 1.1625 | -0.11(3) | -0.13(3) | -0.007(1) | 0.43 |
| 3.2 | 1.1507 | -0.20(3) | -0.22(3) | -0.001(1) | 0.45 |
| 3.6 | 1.1397 | -0.07(6) | -0.08(6) | -0.009(3) | 0.60 |

In Fig. 3 we show two possible fits and their corresponding analytic continuations for the contact, namely Eqs. (14), (15), and an alternative function

$$q(\beta h_{\rm I}) = \gamma \left[ 1 + \mathcal{A}\eta(\beta h_{\rm I}) + \mathcal{B}\eta((\beta h_{\rm I})^3/\pi^2) \right], \qquad (16)$$

where again $\mathcal{A}$ and $\mathcal{B}$ are free real-valued fit parameters and $\gamma$ is a fixed value, as discussed previously. The analytic continuation $\tilde{q}(\beta h)$ is given in terms of $\tilde{\eta}(\beta h)$. While the fits on the imaginary side appear to be of comparable quality, they differ enough in the details that their analytic continuation to the real side displays noticeable discrepancies. This is particularly evident for large $\beta\mu$. We take this to be indicative of the limitations of our approach and it should be viewed as a warning with respect to the choice of the fit function: The Padé form given in Eq. (14) effectively takes into account arbitrarily high powers of $\cos(\beta h_{\rm I})$, whereas the ansatz (16) may be viewed as a low-order approximation of the ansatz (14) in powers of $\cos(\beta h_{\rm I})$ which is expected to be valid only in the vicinity of $\beta h_{\rm I} = 0$. *A priori*, it is difficult to judge under which conditions a low-order approximation is justified at all. In the present case, for example, the value of the coupling does not provide a direct criterion. In fact, already the free Fermi gas in one dimension for $\beta\mu > 0$ is described by an asymptotic series in powers of $\cos(\beta h_{\rm I})$. For $\beta\mu \ll -1$, on the other hand, it can

[1] In higher dimensions, phase transitions may occur, potentially rendering physical quantities non-analytic at the transition point. Depending on the observable and the employed ansatz, such poles may therefore not just be an artifact resulting from the details of the fitting procedure but may be a hint to an underlying physical effect.

Table II. Fit parameters for the magnetization as they appear in Eq. (11) at a constant dimensionless coupling of $\lambda = 1.0$ for various values of $\beta\mu$, as well as the $\chi^2$ per degree of freedom for each fit. The value in parentheses indicates the calculated uncertainty of the least significant digit for each fit parameter.

| $\beta\mu$ | $\mathcal{A}$ | $\mathcal{B}$ | $\mathcal{C}$ | $\chi^2$ |
|---|---|---|---|---|
| -3.6 | 1.022(4) | 0.044(3) | 0.011(5) | 0.48 |
| -3.2 | 1.031(4) | 0.062(3) | 0.011(5) | 0.50 |
| -2.8 | 1.048(3) | 0.094(3) | 0.012(4) | 0.41 |
| -2.4 | 1.047(6) | 0.146(5) | -0.015(6) | 1.01 |
| -2.0 | 1.062(5) | 0.202(4) | -0.023(6) | 1.35 |
| -1.6 | 1.098(4) | 0.269(3) | 0.000(4) | 0.48 |
| -1.2 | 1.134(4) | 0.387(3) | 0.017(4) | 1.80 |
| -0.8 | 1.142(3) | 0.521(3) | 0.037(3) | 5.81 |
| -0.4 | 1.089(4) | 0.632(3) | 0.052(3) | 8.90 |
| 0.0 | 0.978(3) | 0.702(2) | 0.067(2) | 23.32 |
| 0.4 | 0.833(3) | 0.711(3) | 0.088(3) | 36.24 |
| 0.8 | 0.695(3) | 0.684(3) | 0.123(3) | 7.36 |
| 1.2 | 0.574(2) | 0.660(3) | 0.156(3) | 4.95 |
| 1.6 | 0.473(2) | 0.651(3) | 0.175(3) | 7.57 |
| 2.0 | 0.397(2) | 0.639(4) | 0.193(4) | 8.02 |
| 2.4 | 0.340(2) | 0.630(5) | 0.214(5) | 11.10 |
| 2.8 | 0.292(2) | 0.634(6) | 0.215(6) | 14.55 |
| 3.2 | 0.256(1) | 0.638(5) | 0.218(4) | 14.73 |
| 3.6 | 0.227(2) | 0.636(7) | 0.218(7) | 24.89 |

Table III. Fit parameters for the contact as they appear in Eq. (14) at a constant dimensionless coupling of $\lambda = 1.0$ for various values of $\beta\mu$, as well as the $\chi^2$ per degree of freedom for each fit. Note that $\gamma$ is not a fit parameter (see main text). The value in parentheses indicates the calculated uncertainty of the least significant digit for each fit parameter.

| $\beta\mu$ | $\gamma$ | $\mathcal{A}$ | $\mathcal{B}$ | $\mathcal{C}$ | $\chi^2$ |
|---|---|---|---|---|---|
| -3.6 | 0.0003 | -0.4(2) | -0.60(4) | 0.15(4) | 0.47 |
| -3.2 | 0.0019 | -0.50(5) | -0.50(3) | -0.00(5) | 0.52 |
| -2.8 | 0.0062 | -0.503(2) | -0.10(5) | -0.40(8) | 0.12 |
| -2.4 | 0.0159 | -0.5(1) | -0.40(9) | 0.4(6) | 1.01 |
| -2.0 | 0.0390 | -0.45(8) | -0.39(6) | 0.3(4) | 1.30 |
| -1.6 | 0.0971 | -0.5025(5) | -0.22(2) | -0.27(3) | 0.42 |
| -1.2 | 0.1712 | -0.49(1) | -0.42(1) | -0.00(4) | 0.98 |
| -0.8 | 0.3542 | -0.496(2) | -0.418(4) | -0.05(1) | 0.32 |
| -0.4 | 0.5722 | -0.493(2) | -0.473(3) | 0.006(8) | 0.64 |
| 0.0 | 1.0000 | -0.496(1) | -0.464(3) | -0.016(6) | 1.02 |
| 0.4 | 1.4929 | -0.4974(7) | -0.450(2) | -0.029(4) | 0.70 |
| 0.8 | 2.1795 | -0.4978(7) | -0.402(2) | -0.075(4) | 0.60 |
| 1.2 | 2.7994 | -0.494(1) | -0.386(2) | -0.061(6) | 0.49 |
| 1.6 | 3.6330 | -0.4986(7) | -0.331(3) | -0.138(7) | 1.09 |
| 2.0 | 4.3998 | -0.498(1) | -0.304(4) | -0.16(1) | 2.21 |
| 2.4 | 5.0691 | -0.4980(5) | -0.298(2) | -0.157(5) | 0.61 |
| 2.8 | 5.8386 | -0.4975(5) | -0.278(2) | -0.166(5) | 0.53 |
| 3.2 | 6.6344 | -0.4967(7) | -0.256(2) | -0.180(7) | 0.69 |
| 3.6 | 7.3683 | -0.4982(6) | -0.240(2) | -0.211(6) | 0.85 |

be shown that already a low-order approximation yields reliable results for the free Fermi gas, see also our discussion of the virial expansion in Sect. IV B. Apparently, the strength of the coupling does not enter these arguments. A variation of the strength of the coupling is only expected to change the numerical values of the series coefficients associated with such an expansion in powers of $\cos(\beta h_{\mathrm{I}})$ and may therefore only effectively improve or worsen the convergence properties of this series. Note that both limits $\beta\mu \gg 1$ and $\beta\mu \ll -1$ correspond to weak-coupling limits in our Monte Carlo study with fixed dimensionless coupling $\lambda$ and fixed inverse temperature $\beta$. In the regime $|\beta\mu| \lesssim 1$, on the other hand, the theory is effectively in the strongly coupled regime, see also our discussion Sect. IV A.

### C. Magnetization-to-density ratio and magnetic susceptibility

It is important to understand whether the system we are studying is appreciably magnetized in the region of parameter space that we explore here. To clarify this point, in Fig. 4 we show the ratio of the magnetization $m$ to the density $n$. In absolute value, this ratio can only vary between 0 (unpolarized) and 1 (fully polarized). Furthermore, it is reassuring that $m/n$ lies within the interval $[0, 1]$ after analytic continuation, and is a monotonically increasing function with $\beta h$.

Our results for the magnetization allow us to compute the magnetic susceptibility $\chi$ of a polarized Fermi gas

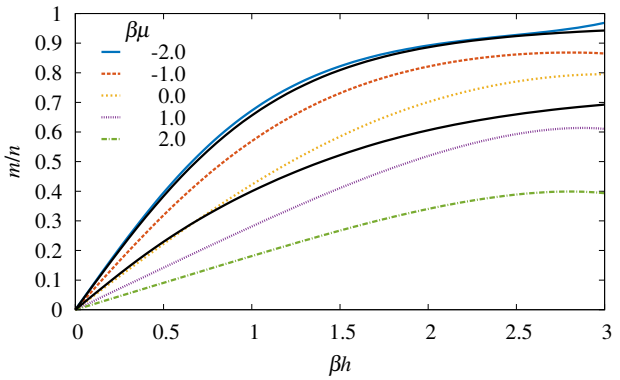


Figure 4. (Color online) Ratio of the magnetization $m$ to the density $n$ as a function of real-valued $\beta h$ and $\beta\mu$ = -2.0, -1.0, 0, 1.0, 2.0. The solid lines show the second-order virial expansion at $\beta\mu = -2$ (top) and -1 (bottom). Note that the virial expansion works well for $\beta\mu = -2$, but fails dramatically for $\beta\mu = -1$ and above; see Section IV B for details.

simply by taking a derivative:

$$\chi = \frac{1}{n_0} \frac{\partial m}{\partial(\beta h)}, \tag{17}$$

where in practice we simply take an analytic derivative of Eq. (13) for each discrete value of $\beta\mu$. The magnetic susceptibility as a function of $\beta h$ for representative values of $\beta\mu$ at a fixed dimensionless coupling of $\lambda = 1.0$, as well as the noninteracting case is shown in Fig. 5.

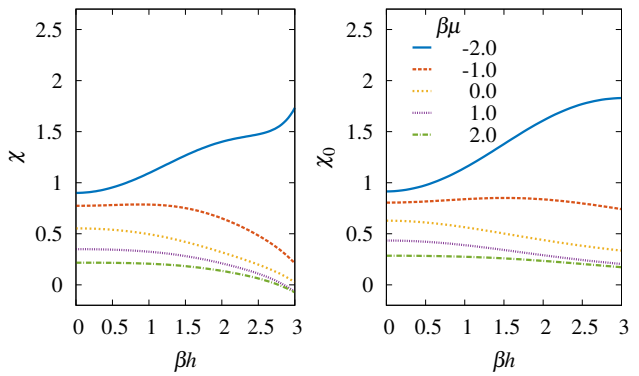


Figure 5. (Color online) The magnetic susceptibility $\chi$ as a function of $\beta h$ at representative values of $\beta\mu$, obtained by taking an analytic derivative of the polarization with respect to $\beta h$. Left panel: interacting case at $\lambda = 1$. Right panel: noninteracting case in the continuum.

Note that the deterioration in the accuracy of the analytic continuation at large $\beta h$ (as discussed in Sec. III B) becomes more apparent as we take derivatives of physical observables.

## IV. COMPARISON WITH OTHER APPROACHES

In this section, we compare the results from our Monte Carlo simulations with those from other approaches which also helped us to guide the analytic continuation of our data from imaginary to real-valued chemical potential differences. Moreover, these comparisons allow us to gain at least some insight into the phenomenology underlying one-dimensional Fermi gases.

### A. Pairing effects

The partition function of the noninteracting gas ($\lambda = 0$) may be computed analytically in the grand-canonical ensemble using

$$\ln \mathcal{Z}(\beta\mu, \beta h) = \frac{L}{\sqrt{\pi}\lambda_T}\left[I_0(z_\uparrow) + I_0(z_\downarrow)\right] , \qquad (18)$$

where

$$I_0(z_s) = \int_{-\infty}^{\infty} dx \ln\left(1 + z_s \mathrm{e}^{-x^2}\right) , \qquad (19)$$

and $z_\uparrow = \mathrm{e}^{\beta\mu}\mathrm{e}^{\beta h}$ and $z_\downarrow = \mathrm{e}^{\beta\mu}\mathrm{e}^{-\beta h}$. From this, it follows immediately that $\ln \mathcal{Z}$ can be written in terms of an asymptotic series of the form

$$\ln \mathcal{Z}(\beta\mu, \beta h) = \sum_{k=0}^{\infty} b_k \mathrm{e}^{k\beta\mu} \cosh(k\beta h) , \qquad (20)$$

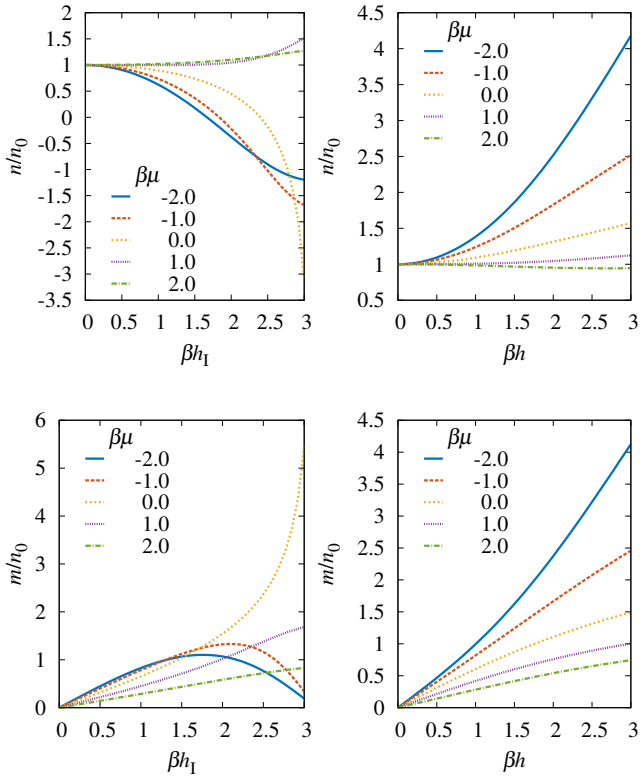


Figure 6. (Color online) Top: Density $n$ of the noninteracting Fermi gas for several values of $\beta\mu$ as a function of imaginary (left panel) and real (right panel) values of $\beta h$. Bottom: Same as top panel, but showing the magnetization $m$. Both $n$ and $m$ are displayed in units of the density $n_0$ of the noninteracting, unpolarized system.

which, in retrospect, motivates our general forms for the ansätze for the fit functions used to analytically continue the Monte Carlo data from imaginary to real-valued chemical potential differences. The coefficients $b_k$ can be related to the one-, two-, three-, ..., $N$-body problem, see also our discussion below. Note that this series converges particularly well for $\beta\mu \ll -1$.

The density and spin magnetization follows immediately from Eq. (18). For the density, we obtain

$$n\lambda_T = \frac{\lambda_T}{L}\frac{\partial \ln \mathcal{Z}(\beta\mu, \beta h)}{\partial(\beta\mu)} = \frac{1}{\sqrt{\pi}}\left[I_1(z_\uparrow) + I_1(z_\downarrow)\right] , \qquad (21)$$

where $I_1(z_s) = z_s \partial I_0(z_s)/\partial z_s$, and, for the magnetization $m$, we find

$$m\lambda_T = \frac{\lambda_T}{L}\frac{\partial \ln \mathcal{Z}(\beta\mu, \beta h)}{\partial(\beta h)} = \frac{1}{\sqrt{\pi}}\left[I_1(z_\uparrow) - I_1(z_\downarrow)\right] . \qquad (22)$$

In Fig. 6, we show our results for the density and the magnetization of the free Fermi gas as a function of $\beta h_\mathrm{I}$ for various values of $\beta\mu$. Comparing these results for the free Fermi gas with those from our Monte Carlo study (see Figs. 1 and 2), we observe that both agree qualitatively,

at least for finite $\beta\mu$. For $\beta\mu = 0$, on the other hand, we observe that the results from the free gas diverge for $|\beta h_{\rm I}| \to \pi$. This can be understood from Eq. (19): Setting $\beta\mu = 0$, we observe that the function $I_0$ diverges at least logarithmically in the limit $|\beta h_{\rm I}| \to \pi$. We would like to add that the reason for the divergence appearing in the results in this limit can also be understood from a study of the free propagator which becomes singular for $\beta\mu = 0$ and $\vec{p}^{\,2} = 0$ in the limit $|\beta h_{\rm I}| \to \pi$. Formulated in the language of thermal field theory, the fermionic Matsubara modes $\beta\omega_n = (2n+1)\pi$ entering the free propagator effectively assume the form $\beta\omega_n = 2n\pi$ associated with bosonic degrees of freedom in the limit $|\beta h_{\rm I}| \to \pi$, see also Ref. [13]. In other words, in this limit the fermions acquire a (thermal) zero mode. However, we emphasize that the partition function is analytic for any finite value of $\beta\mu$.[2] Therefore, no divergences occur in the limit $|\beta h_{\rm I}| \to \pi$ for $\beta\mu \neq 0$. The situation is substantially different in the case of an interacting Fermi gas as studied with our Monte Carlo approach. Here, $\beta\mu$ is only a parameter with limited physical meaning. In fact, whereas $\mu$ determines the energy of the free Fermi gas, the parameter $\mu$ in the Monte Carlo study only sets the scale for the energy of the corresponding interacting Fermi gas. Loosely speaking, an effective chemical potential $\mu_{\rm eff}$ may also be assigned to the interacting Fermi gas. In general, its value would then be different from the value of the parameter $\mu$. Indeed, even for $\beta\mu = 0$, the results for physical observables from our Monte Carlo study appear to be analytic as a function of $\beta h_{\rm I}$. For example, the spin magnetization $m$ diverges for $\beta\mu = 0$ and $|\beta h_{\rm I}| \to \pi$ in the case of the free Fermi gas, see Fig. 6. For the interacting Fermi gas, on the other hand, $m$ appears to be analytic for $\beta\mu = 0$ and only exhibits a rapid decrease in the limit $|\beta h_{\rm I}| \to \pi$, suggesting the effective chemical potential $\mu_{\rm eff}$ associated with the interacting theory is small but finite, see Fig. 2.

Although there is no spontaneous symmetry breaking in one dimension in the long-range limit, pairing of fermions is *a priori* still possible for any finite coupling strength and expected to impact the ground state. It is therefore worthwhile to study pairing in the one-dimensional Fermi gas at zero temperature. In this case, the coupling is conveniently rendered dimensionless with the aid of the chemical potential $\mu$ which sets the scale:

$$\bar{g} = \frac{\lambda}{\sqrt{|\beta\mu|}} = \frac{g}{\sqrt{|\mu|}}\,. \tag{23}$$

Thus, the scale $\beta$ drops out as it should be and the dimensionless coupling $\bar{g}$ can now be viewed as a measure of the potential energy (measured in terms of $g$) relative to the kinetic energy (measured in terms of $\mu$). We observe that, for fixed $\lambda$ and $\beta$ as in our case, we approach the weak-coupling limit for, e.g., $\beta\mu \gg 1$. On the other hand, the theory becomes strongly coupled for fixed $\lambda \sim \mathcal{O}(1)$ if $|\beta\mu| \lesssim 1$.

[2] Note that $\ln \mathcal{Z}$ is a sum of $I_0(e^{\beta\mu}e^{\beta h})$ and $I_0(e^{\beta\mu}e^{-\beta h})$ up to numerical factors.

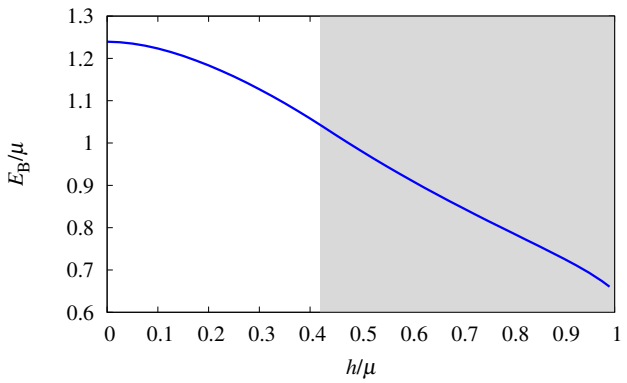


Figure 7. (Color online) Dimensionless binding energy $E_{\rm B}/\mu$ of the two-body bound state in the presence of (inert) Fermi surfaces as a function of $h/\mu$ for $\bar{g} = \pi$. The gray-shaded area depicts the regime in which the formation of a bound state with finite center-of-mass momentum is favored.

Keeping this in mind, let us now analyze the role of pairing effects in our Monte Carlo study by simply considering the two-body problem in the presence of two Fermi surfaces, in close analogy to standard BCS theory [25]. The underlying Schrödinger equation, which has proven very useful to understand the general phase structure of imbalanced Fermi gases [26, 27], is given by

$$\Big[\sum_{s=\uparrow,\downarrow} \epsilon_s(\partial_{x_s}) - g\delta(x_\uparrow - x_\downarrow) + E_{\rm B}\Big]\Psi(x_\uparrow, x_\downarrow) = 0\,. \tag{24}$$

Here, $\Psi$ is the wave-function of the bound state. The operator $\epsilon_s$ is defined as $\epsilon_s(\partial_x) = |-(2m)^{-1}\partial_x^2 - \epsilon_{{\rm F},s}|$ with $\epsilon_{{\rm F},s}$ ($s = \uparrow, \downarrow$) being the Fermi energy of the up- and down-fermions, respectively. Interestingly, the solution of this one-dimensional two-body problem can in principle also be given in closed form [27]. For our purposes, however, only the (binding) energy of the lowest-lying bound-state, which is obtained from a minimization of the energy $E_{\rm B}$ with respect to the total momentum $P$, is of particular interest. For illustration purposes, we show the energy of this state as a function of $h/\mu$ in Fig. 7 for $\bar{g} = \pi$ (in the strong-coupling regime), corresponding to $\beta\mu = 1/\pi^2 \approx 0.1$ in our Monte-Carlo study with fixed $\lambda = 1.0$. The gray-shaded area in Fig. 7 depicts the regime in which it is energetically most favorable to form a bound state with finite center-of-mass momentum. In a full many-body treatment, the true ground state can potentially be inhomogeneous in this regime [26, 27].

We observe that the dimensionless binding energy $E_{\rm B}/\mu$ becomes smaller for increasing spin-imbalance $h/\mu$. Moreover, we find that the formation of a two-body bound state is no longer energetically favored for $\bar{g} \lesssim 0.96$ which corresponds to $\beta\mu \gtrsim 1.08$ in our Monte Carlo study with fixed $\lambda = 1.0$. Loosely speaking, this suggests that, for fixed $\lambda$, the Fermi gas undergoes a crossover from a

strongly correlated to a weakly correlated system in the limit $\beta\mu \gg 1$.

A word of caution needs to be added here: Our study of bound-state formation in the presence of (inert) Fermi surfaces is clearly only an approximation as the Fermi surfaces are smeared out at finite temperature and coupling strength. Moreover, it has been found that the spin-balanced $N_\uparrow + N_\downarrow$-problem "dimerizes", i.e. the ground state energy of this system in the zero-temperature limit is given by the $(N_\uparrow + N_\downarrow)/2$ times the binding energy of the associated two-body bound state (see, e.g., Refs. [8, 28–30]). Thus, even in the limit of small dimensionless coupling $\bar{g}$, bound states are formed. Nevertheless, as in our study of bound-state formation in the presence of Fermi surfaces, the dimensionless energy of the system (i.e. energy measured in units of $\mu$) decreases for fixed coupling $g$ and increasing $\mu$. However, the critical coupling for bound-state formation turns out to be zero in the exact solution, independent of the degree of spin imbalance of the system.

With respect to our Monte Carlo simulations, these considerations imply that pairing effects are present for all values of $\mu$ and $h$ and are at least partly responsible for the difference between the results for the free Fermi gas and our Monte Carlo results. It should also be added that our Monte Carlo study is bound to finite temperature $|\beta h| \leq \pi$ which hinders a direct comparison between our Monte Carlo results and the exact solutions [8, 28] only available for the zero-temperature limit. At finite temperature, thermal energy is "pumped" into the system, effectively resulting in dissociation of the bound states.[3]

We close by adding a comment on local ordering in one-dimensional Fermi gases. The formation of bound states can be considered as a necessary condition for the formation of a superfluid condensate. Of course, as stated above, there is no spontaneous symmetry breaking in these one-dimensional systems in the long-range limit. Nevertheless, the emergence of local ordering, i.e. the emergence of a condensate in the presence of a sufficiently large infrared cutoff, may be possible. In three-dimensional systems, these types of phases are associated with precondensation [27, 31]. In experiments, such an infrared cutoff scale is effectively set by the inverse of the length scale associated with the confining geometry, e.g. a harmonic trap potential. Since the extent of inhomogeneous phases in the space spanned by the experimental parameters is expected to be large [26, 32], it may indeed be worthwhile to further study the fate of these phases at finite temperature with the aid of our present Monte Carlo setup.

[3] Note that our Monte Carlo results are always given as a function of $\beta h$. Thus, large values of $\beta h$ correspond to low temperatures for fixed chemical potential difference $h$, whereas small $\beta h$ is associated with high temperatures in this case.

### B. Virial expansion

Let us now consider the virial expansion of the partition function, i.e. an expansion in powers of $z \equiv \mathrm{e}^{\beta\mu}$. In the $\beta\mu \to -\infty$ limit, where the virial expansion is valid, we can evaluate the density and the magnetization order by order. Indeed, at leading order in $z$, $n_{\uparrow,\downarrow}\lambda_T = z_{\uparrow,\downarrow}$, and therefore

$$n\lambda_T = (n_\uparrow + n_\downarrow)\lambda_T = 2\mathrm{e}^{\beta\mu}\cosh(\beta h) \tag{25}$$

which leads to

$$\frac{n}{n_0} = \cosh(\beta h) \tag{26}$$

where $n_0$ is the density for the unpolarized system. This result is the leading order in the virial expansion and does not depend on the interaction. Similarly, we find for the magnetization that

$$\frac{m}{n_0} = \frac{n_\uparrow - n_\downarrow}{n_0} = \sinh(\beta h)\,, \tag{27}$$

at leading order in $z$ which then yields

$$\frac{m}{n} = \tanh(\beta h)\,, \tag{28}$$

which is valid at the same (leading) order in $z$.

In general, accessing higher orders in the virial expansion requires solving the two-, three-, ..., $N$-body problems (see, e.g., Ref. [33]). The grand-canonical partition function for systems with chemical potential asymmetry may be written as

$$\mathcal{Z} = \sum_{N=0}^{\infty}\sum_{M} z^N w^M Q_{N_\uparrow,N_\downarrow}\,, \tag{29}$$

where $N = N_\uparrow + N_\downarrow$ is the total particle number and $M = N_\uparrow - N_\downarrow$ measures the spin polarization. Moreover, we have introduced the quatitites $w \equiv e^{\beta h}$ and $Q_{N_\uparrow,N_\downarrow}$ being the canonical partition function of a system with $N_\uparrow$ spin-up fermions and $N_\downarrow$ spin-down fermions. Expanding Eq. (29) to second order in $z$ yields

$$\begin{aligned}\mathcal{Z} = 1 &+ 2Q_{1,0}z\cosh(\beta h)\\ &+ Q_{1,1}z^2 + 2Q_{2,0}z^2\cosh(2\beta h) + \mathcal{O}(z^3)\,,\end{aligned} \tag{30}$$

where $Q_{1,0} = L/\lambda_T$ and $Q_{1,1}$ and $Q_{2,0}$ may be determined by direct calculation [24]. Note that the expansion coefficients $Q_{N_\uparrow,N_\downarrow}$ depend implicitly on the coupling $\lambda$. The density $n$ and magnetization $m$ in the second-order virial expansion may then be determined from $\mathcal{Z}$ through Eqs. (21) and (22) and compared with Monte Carlo results in the $z \to 0$ limit. We do this explicitly in Fig. 8 and find excellent agreement for small $z$ and $\beta h$; however, the quality of the agreement deteriorates quickly as $\beta h$ is increased unless $z \simeq 0$, as expected. For completeness, Fig. 9 shows Tan's contact as a function of $\beta\mu$, for several values of $\beta h$, and at $\lambda = 1$.

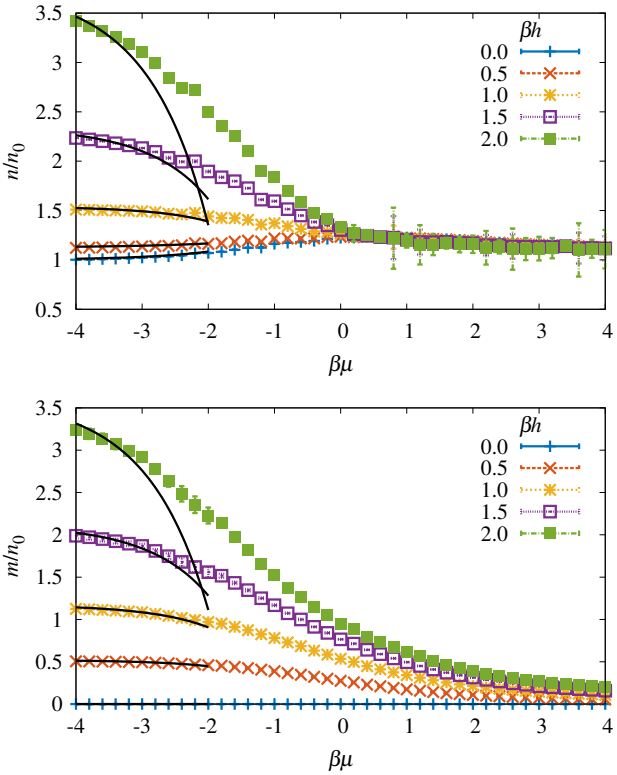


Figure 8. (Color online) Top: Analytic continuation of the density $n$ (in units of its unpolarized, noninteracting counterpart $n_0$) as a function of $\beta\mu$ at a constant coupling $\lambda = 1.0$ and $\beta h = 0$, 0.5, 1.0, 1.5, 2.0. The solid black line shows the second-order virial expansion for each value of $\beta h$. Bottom: Same as top, but showing the magnetization $m$. Error bars were estimated by varying the fit parameters by an amount given by the uncertainty in the calculated fits.

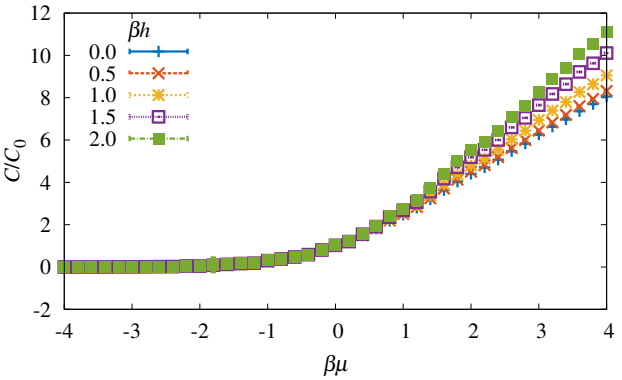


Figure 9. (Color online) Analytic continuation of Tan's contact as a function of $\beta\mu$ at a constant coupling $\lambda = 1.0$ and $\beta h = 0$, 0.5, 1.0, 1.5, 2.0. The statistical error is on the order of the size of the plotted symbol. $C_0$ is the contact at $\beta\mu = \beta h = 0$.

### C. Lattice perturbation theory

As an additional verification of the equations of state obtained through an analytic continuation, we performed a next-to-leading order lattice perturbation theory calculation by expanding the lattice grand-canonical partition function $\mathcal{Z}(\beta\mu, \beta h)$ in the dimensionless parameter $A \equiv \sqrt{2(e^{\tau g} - 1)}$ (which arises naturally in lattice calculations, see Ref. [17]) about the noninteracting limit ($A = 0$), up to the second non-vanishing term. Such an expansion on the lattice yields

$$\ln \mathcal{Z} = \ln \mathcal{Z}_0 + \frac{\beta}{2\tau N_x}(Ae^{\beta\mu})^2 \prod_{s=\uparrow,\downarrow}\left(\sum_k \frac{e^{-\beta\epsilon_k}}{1 + z_s e^{-\beta\epsilon_k}}\right), \tag{31}$$

where $\mathcal{Z}_0(\beta\mu, \beta h)$ is the partition function of the noninteracting gas, $\epsilon_k = k^2/2m$ and the sum over $k$ is over all possible lattice momenta. The density $n/n_0$ and magnetization $m/n_0$ in terms of this perturbation theory therefore follow from Eq. (31) using Eqs. (21) and (22). We display the results of this analytic calculation with the numerical Monte Carlo results and the equations of state of the free gas in Fig. 10. In all cases the results obtained with our proposed analytic-continuation approach lie generally between the leading (noninteracting) calculation and the next-to-leading-order result.

## V. SUMMARY AND CONCLUSIONS

In summary, we have performed a non-perturbative characterization of the density $n$, magnetization $m$, magnetic susceptibility $\chi$, and Tan's contact $C$ of a 1D, attractively interacting Fermi gas. To this end, we implemented the conventional finite-temperature lattice Monte Carlo formalism, but generalized to include complex chemical potentials. When the chemical potential asymmetry $h$ is purely imaginary, there is no sign problem and the Monte Carlo calculation can be carried out as usual. Our Monte Carlo results on the imaginary-$h$ side are therefore exact up to controlled (statistical and systematic) uncertainties.

To obtain results for real $h$, we performed fits to our numerical data and implemented an analytic continuation, i.e. we set $h \to ih$. In some regions of parameter space, different functional forms for the fits may yield very different analytic continuations. However, very simple functional forms such as polynomials can be discarded as they are likely too simple to capture the essential physics. Generally speaking, at low enough $\beta h$ all fits lead to (approximately) the same analytic continuation. As we show in Fig. 4, however, even for low $\beta h$, we achieve non-trivial magnetization ratios as large as $m/n \simeq 0.3 - 0.5$.

We have presented our results as a function of the dimensionless parameters $\beta\mu$ and $\beta h$, but focused on an intermediate- to strong-coupling regime $\lambda = \sqrt{\beta}g \sim \mathcal{O}(1)$ as a non-trivial case of relevance for future studies. Our results for $n$ and $m$ agree qualitatively with the free Fermi gas where differences may be traced back to pair-

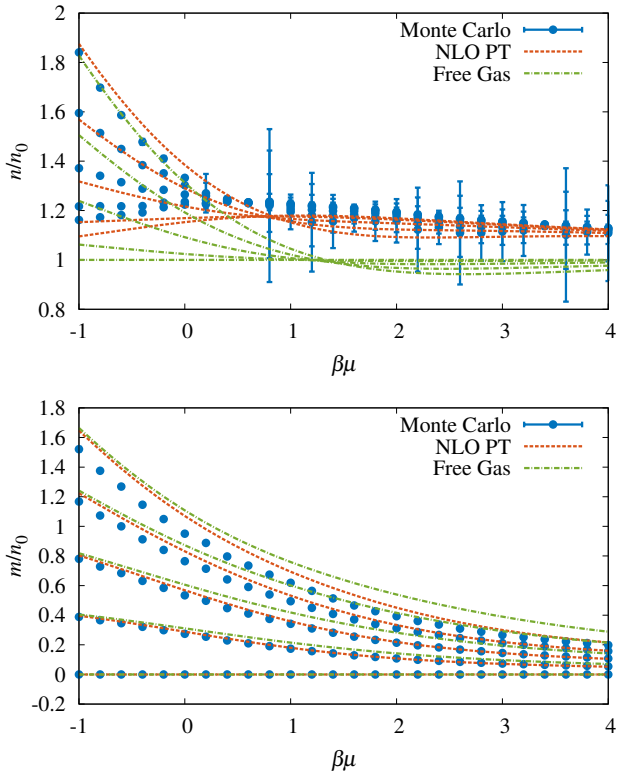


Figure 10. (Color online) Comparison of the Monte Carlo results after the analytic continuation, a next-to-leading order perturbation theory calculation (NLO PT), and the free gas for the density (top) and the magnetization (bottom). Results are displayed for $\beta h = 0.0, 0.5, 1.0, 1.5$ and 2.0 (bottom to top) in the strongly interacting region $\beta\mu > -1$.

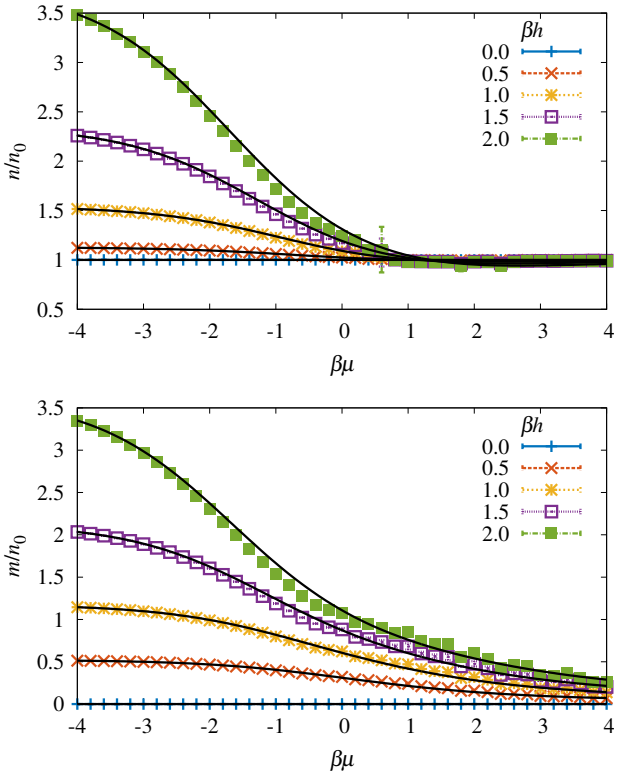


Figure 11. (Color online) Analytic continutation of the density (top) and the magnetization (bottom) for the non-interacting system as a function of $\beta\mu$ for various values of $\beta h$. The exact solutions in the continuum limit are shown as solid black lines.

ing effects. Moreover, our results are consistent with the second-order virial expansion, which is non-perturbative in the interaction, in the regime $\beta\mu < 0$, where that expansion is valid. We also note, however, that the virial expansion deteriorates as $\beta h$ is increased (at fixed $z$).

The calculations carried out in this work correspond to fixed lattice volume $L = N_x\ell = 61$ and extent of the imaginary-time direction $\beta = N_\tau\tau = 8.0$, where $\ell = 1$ and $\tau = 0.05$. The associated systematic effects should, in principle, be further investigated, although the results of our previous work [24] indicate that those effects are below 10%. We consider our present work as a proof-of-principle study of our imaginary spin-imbalance approach. However, results for, e.g., the thermal equations of state, could already be extracted from it and compared to present and future experiments [18], if available. In any case, our present study is mostly aimed at paving the way to more computationally demanding systems in two and three dimensions. For example, our approach allows one to map out to some extent the finite-temperature phase diagram of spin-imbalanced unitary Fermi gases in three dimensions, and therefore permits one to, at least, narrow down the regime in parameter space in which the critical point is located. In that regard, all of our present results indicate that calculations in higher dimensions should be feasible with the proposed method.

## ACKNOWLEDGMENTS

We thank W. J. Porter, and L. Rammelmüller for useful discussions. J.B. and D.R. acknowledge support by the DFG under Grant BR 4005/2-1 and by HIC for FAIR within the LOEWE program of the State of Hesse. This material is based upon work supported by the National Science Foundation Graduate Research Fellowship Program under Grant No. DGE1144081, National Science Foundation Nuclear Theory Program under Grant No. PHY1306520, National Science Foundation Computational Physics Program under Grant No. PHY1452635, and National Science Foundation REU Sites Program under Grant No. ACI1156614.

Table IV. Fit parameters for the density at alternative coupling strengths for various values of $\beta\mu$, as well as the $\chi^2$ per degree of freedom for each fit. Note that $\gamma$ is not a fit parameter (see main text). The value in parentheses indicates the calculated uncertainty of the least significant digit for each fit parameter.

| $\lambda$ | $\beta\mu$ | $\gamma$ | $\mathcal{A}$ | $\mathcal{B}$ | $\mathcal{C}$ | $\chi^2$ |
|---|---|---|---|---|---|---|
| 0.5 | -2.0 | 1.0272 | -0.8876(3) | -0.1553(7) | -0.0029(7) | 1.45 |
| 0.5 | -1.0 | 1.0624 | -0.7412(8) | -0.299(2) | -0.027(2) | 2.63 |
| 0.5 | 0.0 | 1.0937 | -0.5216(4) | -0.392(3) | -0.064(4) | 2.21 |
| 0.5 | 1.0 | 1.1018 | -0.2(3) | -0.2(3) | -0.05(6) | 0.73 |
| 0.5 | 2.0 | 1.0908 | -0.20(2) | -0.23(2) | -0.014(2) | 0.64 |
| 2.0 | -2.0 | 1.2530 | -0.712(2) | -0.163(7) | -0.007(9) | 0.69 |
| 2.0 | -1.0 | 1.5051 | -0.483(6) | -0.278(8) | 0.11(6) | 1.97 |
| 2.0 | 0.0 | 1.6588 | -0.502(2) | -0.491(2) | -0.012(1) | 0.98 |
| 2.0 | 1.0 | 1.5738 | -0.35(5) | -0.37(5) | 0.006(1) | 1.78 |
| 2.0 | 2.0 | 1.4263 | -0.17(5) | -0.18(5) | 0.005(1) | 1.14 |

Table V. Fit parameters for the magnetization at alternative coupling strengths for various values of $\beta\mu$, as well as the $\chi^2$ per degree of freedom for each fit. The value in parentheses indicates the calculated uncertainty of the least significant digit for each fit parameter.

| $\lambda$ | $\beta\mu$ | $\mathcal{A}$ | $\mathcal{B}$ | $\mathcal{C}$ | $\chi^2$ |
|---|---|---|---|---|---|
| 0.5 | -2.0 | 1.082(2) | 0.193(2) | 0.000(3) | 0.72 |
| 0.5 | -1.0 | 1.170(3) | 0.464(3) | 0.020(3) | 3.84 |
| 0.5 | 0.0 | 1.109(3) | 0.778(2) | 0.094(2) | 26.24 |
| 0.5 | 1.0 | 0.770(9) | 0.708(9) | 0.186(8) | 756.92 |
| 0.5 | 2.0 | 0.487(7) | 0.64(1) | 0.25(1) | 458.75 |
| 2.0 | -2.0 | 1.069(5) | 0.179(4) | 0.010(6) | 0.51 |
| 2.0 | -1.0 | 1.023(8) | 0.392(7) | 0.027(8) | 1.57 |
| 2.0 | 0.0 | 0.719(4) | 0.539(4) | 0.049(5) | 6.39 |
| 2.0 | 1.0 | 0.422(2) | 0.562(3) | 0.093(4) | 9.16 |
| 2.0 | 2.0 | 0.265(1) | 0.586(3) | 0.115(3) | 16.25 |

## Appendix A: Analytic continuation of the non-interacting system

In order to verify that the approach of analytically continuing the equations of state of the density $n/n_0$ and magnetization $m/n_0$ is valid using the fit ansätze developed in the main text, we have performed the same prescription for the non-interacting polarized Fermi gas and compared with the exact solution for these quantities in the continuum limit. The results comparing the Monte Carlo and analytic solutions are shown in Fig. 11. There is excellent agreement between the two calculations within systematic and statistical error, which demonstrates a measure of validity for the analytic continution in the interacting case. In the limit of $\lambda \to 0$ on the imaginary side, $m(\beta h_{\rm I})/n_0$ converges to a sawtooth wave of periodicity $2\pi$ for large positive $\beta\mu$, whose behavior in the vicinity of $\beta h_{\rm I} = \pm\pi$ is difficult to capture for the given ansatz. As such, the determined fit parameters $\mathcal{A}$, $\mathcal{B}$, and $\mathcal{C}$ are not necessarily smooth functions of $\beta h_{\rm I}$, and noise is introduced into the result for $m(\beta\mu)/n_0$. The smoothness of the interacting results shown in the main text for $\lambda > 0$ significantly reduces such effects.

## Appendix B: Equations of state for alternative coupling strengths

In the main text we have illustrated the method of calculating the equation of state of polarized, interacting fermions using complex chemical potentials at a constant coupling of $\lambda = 1.0$ for clarity and as a proof of principle. This same method can be applied to other values of the coupling as well, considering that larger values of $\lambda$ may require a larger number of Monte Carlo samples in order to mantain the statistical quality of the data. In Figs. 12 and 13 we show the density and magnetization as functions of both $\beta h$ and $\beta h_{\rm I}$ for dimensionless couplings $\lambda = 0.5$ and 2.0. The fit parameters for a chosen set of $\beta\mu$ at these couplings are provided in Tables IV and V.

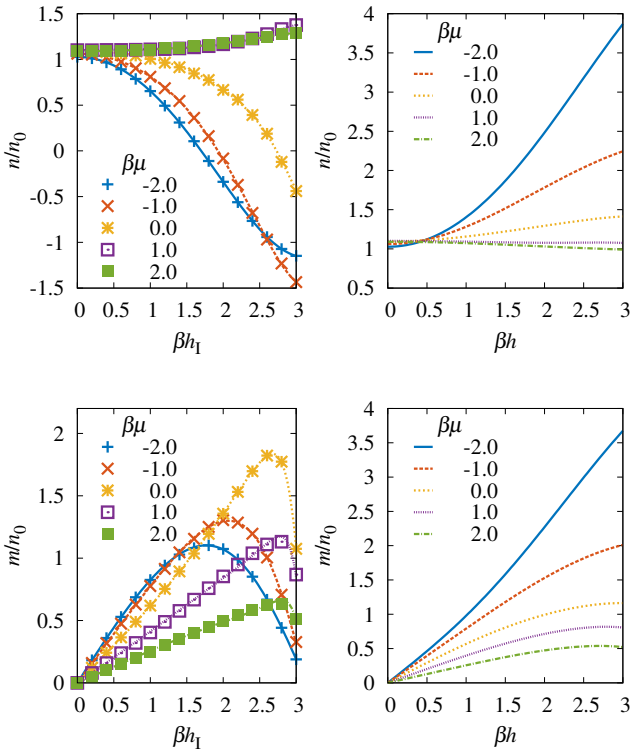


Figure 12. (Color online) Top: Density at a decreased coupling strength of $\lambda = 0.5$ as a function of the imaginary chemical potential difference $\beta h_{\rm I}$ (left) and its analytic continuation to $\beta h$ (right). Bottom: Magnetization at a decreased coupling strength of $\lambda = 0.5$ as a function of the imaginary chemical potential difference $\beta h_{\rm I}$ (left) and its analytic continuation to $\beta h$ (right).

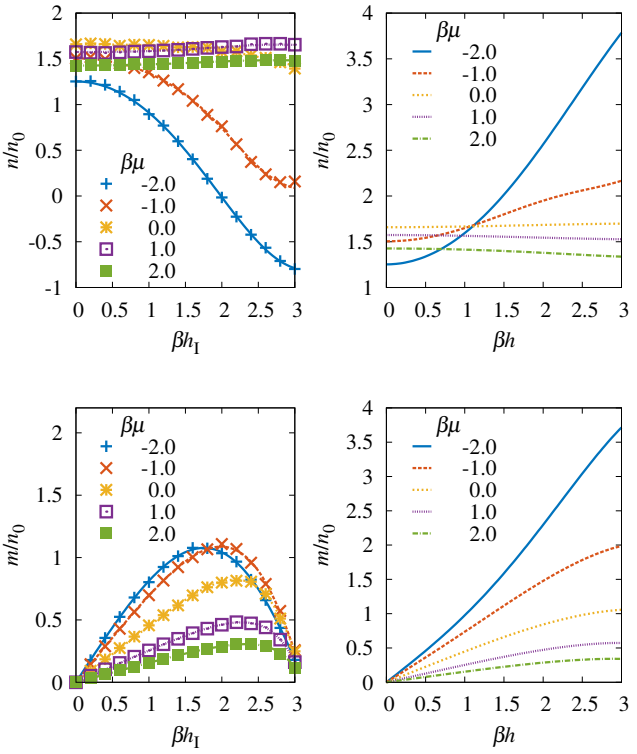


Figure 13. (Color online) Top: Density at an increased coupling strength of $\lambda = 2.0$ as a function of the imaginary chemical potential difference $\beta h_{\rm I}$ (left) and its analytic continuation to $\beta h$ (right). Bottom: Magnetization at a increased coupling strength of $\lambda = 2.0$ as a function of the imaginary chemical potential difference $\beta h_{\rm I}$ (left) and its analytic continuation to $\beta h$ (right).


[1] *Ultracold Fermi Gases*, Proceedings of the International School of Physics "Enrico Fermi", Course CLXIV, Varenna, June, 2006, edited by M. Inguscio, W. Ketterle, and C. Salomon (IOS, Amsterdam, 2008).

[2] I. Bloch, J. Dalibard, and W. Zwerger, Rev. Mod. Phys. **80**, 885 (2008); S. Giorgini, L. P. Pitaevskii, and S. Stringari, *ibid* **80**, 1215 (2008).

[3] *The BCS-BEC Crossover and the Unitary Fermi Gas*, edited by W. Zwerger (Springer-Verlag, Berlin, 2012).

[4] E. Braaten and H.-W. Hammer, Phys. Rep. **428**, 259 (2006); F. Ferlaino and R. Grimm, Physics **3**, 9 (2010).

[5] J. Levinsen, M. M. Parish, Annu. Rev. Cold Atoms Mol. **3**, 1 (2015).

[6] *40 Years of Berezinskii-Kosterlitz-Thouless Theory* , edited by J.V. Jose (World Scientific, Singapore, 2013); V. L. Berezinskii, Sov. Phys. JETP **34**, 610 (1972); J. M. Kosterlitz and D.J. Thouless, J. Phys. C **6**, 1181 (1973); J. M. Kosterlitz, *ibid.* **7**, 1046 (1974).

[7] X-W. Guan, M. T. Batchelor, and C. Lee Rev. Mod. Phys. **85**, 1633 (2013).

[8] M. Takahashi, Prog. Theor. Phys. **44**, 348 (1970); *Thermodynamics of One-Dimensional Solvable Models* (Cambridge University Press, Cambridge, 1999); T. Giamarchi, *Quantum Physics in One Dimension*, (Oxford University Press, Oxford, 2004).

[9] L. Amico, R. Fazio, A. Osterloh, and V. Vedral, Rev. Mod. Phys. **80**, 517 (2008). R. Horodecki, P. Horodecki, M. Horodecki, K. Horodecki, *ibid.* **81**, 865 (2009); J. Eisert, M. Cramer and M. B. Plenio, *ibid.* **82**, 277 (2010)

[10] A. I. Larkin and Yu. N. Ovchinnikov, Zh. Eksp. Teor. Fiz. **47**, 1136 (1964) [Sov. Phys. JETP **20**, 762 (1965)]; P. Fulde and R. A. Ferrell, Phys. Rev. **135**, A550 (1964).

[11] S. Tan, Ann. Phys. **323**, 2952 (2008); *ibid.* **323**, 2971 (2008); *ibid.* **323**, 2987 (2008); S. Zhang, A. J. Leggett, Phys. Rev. A **77**, 033614 (2008); F. Werner, *ibid.* **78**, 025601 (2008); E. Braaten, L. Platter, Phys. Rev. Lett. **100**, 205301 (2008); E. Braaten, D. Kang, L. Platter, *ibid.* **104**, 223004 (2010); C. Langmack, M. Barth, W. Zwerger, E. Braaten, *ibid.* **108**, 060402 (2012). J.E. Drut, T.A. Lähde, T. Ten, *ibid.* **106**, 205302 (2011); K. Van Houcke, F. Werner, E. Kozik, N. Prokof'ev, B. Svistunov, arXiv:1303.6245.

[12] F. Werner and Y. Castin, Phys. Rev. A **86**, 013626 (2012). E. Braaten, in *The BCS-BEC Crossover and the*

*Unitary Fermi Gas*, edited by W. Zwerger (Springer-Verlag, Berlin, 2012); M. Valiente, N. T. Zinner, and K. Mølmer, Phys. Rev. A **84**, 063626 (2011); Phys. Rev. A **86**, 043616 (2012).

[13] J. Braun, J.-W. Chen, J. Deng, J. E. Drut, B. Friman, C.-T. Ma, and Y.-D. Tsai, Phys. Rev. Lett. **110**, 130404 (2013); D. Roscher, J. Braun, J.-W. Chen, and J. E. Drut, J. Phys. G: Nucl. Part. Phys. **41**, 055110 (2014).

[14] J. Braun, J. E. Drut, and D. Roscher, Phys. Rev. Lett. **114**, 050404 (2015).

[15] M. G. Alford, A. Kapustin and F. Wilczek, Phys. Rev. D **59**, 054502 (1999); P. de Forcrand and O. Philipsen, Nucl. Phys. **B642**, 290 (2002); M. D'Elia and M.-P. Lombardo, Phys. Rev. D **67**, 014505 (2003); F. Karbstein and M. Thies, *ibid.* **75**, 025003 (2007); M. P. Lombardo, PoS (**CPOD2006**) 003; P. Cea, L. Cosmai, M. D'Elia, C. Manneschi and A. Papa, Phys. Rev. D **80**, 034501 (2009).

[16] M. Gaudin, Phys. Lett. **24**A, 55 (1967); C.N. Yang, Phys. Rev. Lett. **19**, 1312 (1967).

[17] F. F. Assaad and H. G. Evertz, Worldline and Determinantal Quantum Monte Carlo Methods for Spins, Phonons and Electrons, in *Computational Many-Particle Physics*, edited by H. Fehske, R. Shnieider, and A. Weise (Springer, Berlin, 2008); D. Lee, Phys. Rev. C **78**, 024001 (2008); Prog. Part. Nucl. Phys. **63**, 117 (2009); J. E. Drut and A. N. Nicholson, J. Phys. G **40**, 043101 (2013).

[18] H. Moritz, T. Stöferle, K. Güenter, M. Köhl, and T. Esslinger, Phys. Rev. Lett. **94**, 210401 (2005); Liao, Y.-A., Rittner, A. S. C., Paprotta, T., et al., Nature (London) **467**, 567 (2010); G. Zürn, A. N. Wenz, S. Murmann, A. Bergschneider, T. Lompe, and S. Jochim Phys. Rev. Lett. **111**, 175302 (2013).

[19] N. D. Mermin, H. Wagner, Phys. Rev. Lett. **17**, 1133 (1966); P. C. Hohenberg, Phys. Rev. **158**, 383 (1967); S. Coleman, Commun. Math. Phys. **31**, 259 (1973).

[20] V. E. Barlette, M. M. Leite, S. K. Adhikari, Eur. J. Phys., **21** 435 (2000).

[21] A. Bulgac, J. E. Drut, and P. Magierski, Phys. Rev. Lett. **96**, 090404 (2006).

[22] A. Bulgac, J. E. Drut, and P. Magierski, Phys. Rev. A **78**, 023625 (2008).

[23] J. E. Drut, T. A. Lähde, G. Wlazlowski, P. Magierski, Phys. Rev. A **85**, 051601(R) (2012).

[24] M. D. Hoffman, P. D. Javernick, A. C. Loheac, W. J. Porter, E. R. Anderson, and J. E. Drut, Phys. Rev. A **91**, 033618 (2015).

[25] Leon N. Cooper, Phys. Rev. **104**, 1189 (1956).

[26] D. Roscher, J. Braun and J. E. Drut, Phys. Rev. A **89**, no. 6, 063609 (2014);

[27] D. Roscher, J. Braun and J. E. Drut, Phys. Rev. A **91**, no. 5, 053611 (2015).

[28] J. B. McGuire, J. Math. Phys. **7**, 123 (1966).

[29] L. Rammelmüller, W. J. Porter, A. C. Loheac and J. E. Drut, Phys. Rev. A **92**, 013631 (2015).

[30] T. Grining, M. Tomza, M. Lesiuk, *et al.*, arXiv:1507.03174.

[31] A. R. Sá de Melo, M. Randeria, and J. R. Engelbrecht, Phys. Rev. Lett. **71**, 3202 (1993); M. Randeria and N. Trivedi, Journal of Physics and Chemistry of Solids **59**, 1754 (1998); J. P. Gaebler, J. T. Stewart, T. E. Drake, D. S. Jin, A. Perali, P. Pieri, and G. C. Strinati, Nat. Phys. **6**, 569 (2010); A. Perali, F. Palestini, P. Pieri, G. C. Strinati, J. T. Stewart, J. P. Gaebler, T. E. Drake, and D. S. Jin, Phys. Rev. Lett. **106**, 060402 (2011); E. Mueller, Phys. Rev. A 83, 053623 (2011); I. Boettcher, J. M. Pawlowski, and S. Diehl, Nucl. Phys. B - Proc. Suppl. **228**, 63 (2012); Y. Sagi, T. E. Drake, R. Paudel, R. Chapurin, and D. S. Jin, Phys. Rev. Lett. **114**, 075301 (2015); I. Boettcher, J. Braun, T. K. Herbst, J. M. Pawlowski, D. Roscher and C. Wetterich, Phys. Rev. A **91**, no. 1, 013610 (2015).

[32] K. Yang, Phys. Rev. B **63**, 140511(R) (2001); M. M. Parish, S. K. Baur, E. J. Mueller, D. A. Huse, Phys. Rev. Lett. **99**, 250403 (2007); G. Orso, *ibid.* **98**, 070402 (2007); H. Hu, X.-J. Liu, P. D. Drummond, *ibid.* **98**, 070403 (2007); A. E. Feiguin, F. Heidrich-Meisner, Phys. Rev. B **76**, 220508(R) (2007); M. Tezuka, M. Ueda, Phys. Rev. Lett. **100**, 110403 (2008); G. G. Batrouni, M. J. Wolak, F. Hebert, V. G. Rousseau, Europhys. Lett. **86**, 47006 (2009); M. Casula, D. M. Ceperley, E. J. Mueller, Phys. Rev. A **78**, 033607 (2008); B. Wang, Han-Dong Chen, S. Das Sarma, *ibid.* **79**, 051604(R) (2009).

[33] X.-J. Liu, Phys. Rep. **524**, 37 (2013).